

INTERVAL-BASED REDUCED-ORDER MODELS FOR UNSTEADY FLUID FLOW

JEFF BORGGAARD, ALEXANDER HAY, AND DOMINIQUE PELLETIER

This paper is dedicated to Max Gunzburger on the occasion of his 60th birthday

Abstract. A number of practical engineering problems require the repeated simulation of unsteady fluid flows. These problems include the control, optimization and uncertainty quantification of fluid systems. To make many of these problems tractable, reduced-order modeling has been used to minimize the simulation requirements. For nonlinear, time-dependent problems, such as the Navier-Stokes equations, reduced-order models are typically based on the proper orthogonal decomposition (POD) combined with Galerkin projection. We study several modifications to this reduced-order modeling approach motivated by the optimization problem underlying POD. Our discussion centers on a method known as the principal interval decomposition (PID) due to IJzerman.

Key Words. reduced-order modeling, proper orthogonal decomposition, principal interval decomposition, surrogate model, optimization.

1. Introduction

The use of reduced-order modeling in control and optimization has led to practical solutions for extremely challenging problems, such as control of high-Reynolds number flow [29], solutions to the Hamilton-Jacobi-Bellman equation arising in nonlinear feedback control [21], and design of materials for desired microstructure-sensitive material properties [10]. The development of accurate and reliable reduced-order models is critical to the success of these solution approaches. In this paper, we discuss reduced-order models for unsteady flows and suggest a number of potential improvements.

As in the examples above, reduced-order modeling for nonlinear, time-dependent problems typically consists of a basis selection strategy coupled with a model building step. This usually involves a proper orthogonal decomposition (POD) [22] of simulation time snapshots followed by Galerkin projection to build the model (cf. [13] and [1]). The POD and its variants are also known as Karhunen-Loève expansions [19, 22], principal component analysis (PCA) [14], and empirical orthogonal functions (EOF) [23] among others. This method of coupling a reduced-basis with Galerkin projection to build reduced-order models of fluid flow has developed over the past two decades [28] as more complex simulation [26] and control [17] applications emerged. However, reduced-order modeling remains both a “science” and

Received by the editors February 27, 2006.

2000 *Mathematics Subject Classification.* 37N10, 76D55, 76M25.

This research was supported in part by the Air Force Office of Scientific Research (under contract FA9550-05-1-0449), the National Science Foundation (under contract DMS-0513542), the National Science and Engineering Council of Canada, and the Canada Research Chair Program.

an “art.” There are examples where POD combined with Galerkin projection can produce unstable models from stable, linear systems [33]. Thus, there is an industry in constructing new approaches for reduced-order modeling of both linear and nonlinear systems.

A number of improvements to the basis selection and model building have been suggested over the past two decades. Improvements to the Galerkin model-building portion include the theoretically promising, nonlinear Galerkin methods [24] have not proven to be a practical alternative to the standard Galerkin methods [18, 20]. However, for flow problems, a number of specialized approaches have shown promise in managing the energy decay in the model. These are based on modifying or tuning the viscosity term in the model [6, 9, 31].

To develop adequate basis functions from POD, a (number of) representative simulation(s) (known as an input collection) is needed. This frequently requires input from a disciplinary specialist although a number of heuristics based on the spectral content of the input collection have been suggested, eg. [8]. As well shall see, the standard application of POD can miss flow structures that are dynamically relevant but are only expressed for small time intervals. Problems with a convective nature (eg. travelling waves) produce POD bases that don’t capture any problem solution structure. This can prevent adequate dimension reduction.

Recent approaches consider the simultaneous calculation of the basis and the model [32, 2]. In this paper, we consider the little known principal interval decomposition (PID) [16] and some new extensions. The PID simultaneously finds a basis element and the time interval over which it is expressed in the data. Thus, it is well suited for convective problems. In a number of natural extensions to the PID, we consider multiple basis elements per time interval as well as comment on practical criteria for choosing the length of the time interval. The result of this last modification is the development of an *a priori* estimate of the error associated with the resulting PID/Galerkin model. Numerical experiments involving the unsteady von Karman vortex shedding past a square cylinder demonstrate the effectiveness of these modifications.

2. Overview of reduced-order modeling

We begin by giving an overview of the POD/Galerkin framework for reduced-order modeling in this section. This will provide the context and notation to explain the PID approaches in the next section. To facilitate this overview, consider the (two-dimensional, incompressible) Navier-Stokes equations

$$\begin{aligned} (1) \quad \mathbf{u}_t + \mathbf{u} \cdot \nabla \mathbf{u} &= -\nabla p + \nabla \cdot \boldsymbol{\tau}(\mathbf{u}) + \mathbf{f} \\ (2) \quad \nabla \cdot \mathbf{u} &= 0 \end{aligned}$$

where $\mathbf{u} = (u, v)$ is the velocity vector, p is the pressure, $\boldsymbol{\tau}(\mathbf{u}) = 2\nu\boldsymbol{\varepsilon}(\mathbf{u})$ is the deviatoric fluid stress tensor, ν is the kinematic viscosity, and $\boldsymbol{\varepsilon}(\mathbf{u}) = 1/2(\nabla\mathbf{u} + \nabla\mathbf{u}^T)$ is the symmetric strain-rate tensor. With suitable nondimensionalization, ν is the reciprocal of the Reynolds number.

An important step in reduced-order modeling is to find a suitable set of basis functions. We will give an overview of methods to find them below. For now, assume we have a reduced-basis of dimension r , $\{\phi_j(\cdot)\}_{j=1}^r$ with $\phi_j(\cdot) \in [H^1(\Omega)]^2$ where Ω is the flow domain. Using this basis, we represent our reduced-order approximation

to the velocity vector as

$$(3) \quad \mathbf{u}^r(x, t) = \sum_{j=1}^r \phi_j(x) a_j(t) \in P^r \equiv \text{span} \{ \phi_j \}_{j=1}^r$$

and develop a differential equation for the coefficients $\{a_j(\cdot)\}_{j=1}^r$ by a Galerkin projection.

Using the weak form of (1)-(2), cf. [11], we seek $\mathbf{u} \in \mathbf{X} = [H^1]^2$ and $p \in L_0^2$ such that

$$(4) \quad (\mathbf{u}_t, \mathbf{v}) + (\mathbf{u} \cdot \nabla \mathbf{u}, \mathbf{v}) = -(\nabla p, \mathbf{v}) - (\boldsymbol{\tau}(\mathbf{u}) : \boldsymbol{\epsilon}(\mathbf{u})), \quad \mathbf{v} \in \mathbf{X}$$

$$(5) \quad (\nabla \cdot \mathbf{u}, q) = 0 \quad q \in L_0^2.$$

If we have the property that $P^r \subset \mathbf{X}_{\text{div}}$, then we can ignore the pressure term in (4) and equation (5). Thus, ordinary differential equations for $\{a_j\}$ are obtained by substitution of expression (3) into

$$(\mathbf{u}_t^r, \phi_i) = -(\mathbf{u}^r \cdot \nabla \mathbf{u}^r, \phi_i) - (\boldsymbol{\tau}(\mathbf{u}^r) : \boldsymbol{\epsilon}(\phi_i))$$

for $i = 1, \dots, r$. We denote this autonomous set of r equations by

$$(6) \quad E\dot{\mathbf{a}}(t) = f(\mathbf{a}(t)), \quad t \in (0, T), \quad \mathbf{a}_i(0) = (\mathbf{u}, \phi_i)$$

for $i = 1, \dots, r$ where $E_{ij} = (\phi_j, \phi_i)$.

Note that frequently, we have a good approximation for \mathbf{u} at hand. Possibilities include

- a simplified model, eg. potential flow,
- a solution from a coarser mesh,
- a time average of the flow, or a steady-state flow.

We denote this approximation by $\mathbf{c}(x, t)$ and refer to this as a centering trajectory (frequently called a shift-mode or wake-mode in the literature [25]). In this case, we define

$$(7) \quad \mathbf{u}^r(x, t) = \mathbf{c}(x, t) + \sum_{j=1}^r \phi_j(x) a_j(t)$$

and seek an approximation for the correction term, $\mathbf{u} - \mathbf{c}$.

2.1. Basis selection by the proper orthogonal decomposition. The ability of the reduced-order model to approximate the result from a full-order simulation well, critically depends on the basis that is used in (3) or (7). Thus, there is an underlying assumption in reduced-order modeling that the dynamics of $\mathbf{u}(x, t)$ or the discrepancy $\mathbf{u}(x, t) - \mathbf{c}(x, t)$ can be well represented by a reduced-basis. A natural way to find this basis, is to find basis elements that are well expressed over a collection of “typical” simulations. The choice of this so-called *input collection* of simulation data is an art that is inherently discipline specific, though can be guided by mathematics and statistics. For this discussion, we will assume the input collection is the result of a single full-order simulation (which we will denote by $\mathbf{y}(x, t) = \mathbf{u}(x, t)$ or $\mathbf{y}(x, t) = \mathbf{u}(x, t) - \mathbf{c}(x, t)$).

The natural way to introduce the proper orthogonal decomposition is to define the first basis function as

$$\phi_1 = \max_{\|\phi\|=1} \left\{ \frac{1}{T} \int_0^T (\mathbf{y}(\cdot, t), \phi(\cdot))^2 dt \right\}.$$

Thus, ϕ_1 is a basis element that maximizes the time-averaged projection onto the data \mathbf{y} . In some disciplines, this quantity has a physical interpretation of

energy, so this projection is sometimes referred to as the *POD energy*. The second basis function ϕ_2 is that which maximizes the POD energy over the orthogonal complement to ϕ_1 . Subsequent basis functions are defined similarly.

A necessary condition for this optimization problem is that each ϕ_i solve the following eigenvalue problem [13]:

$$\int_{\Omega} R^s(x, \bar{x}) \phi(\bar{x}) d\bar{x} = \lambda \phi(x), \quad \text{for } x \in \Omega,$$

where

$$R^s(x, \bar{x}) = \frac{1}{T} \int_0^T \mathbf{y}(t, x) \mathbf{y}^*(t, \bar{x}) dt$$

is known as the *spatial autocorrelation function*. If our data, $\mathbf{y} \in L^2(0, T; L^2(\Omega))$ (which may require special properties of \mathbf{c}), then R^s is the kernel of a compact, normal operator \bar{R} [13] which leads to a number of useful properties. For real data, the eigenvalue problems are real, the point spectrum of \bar{R} is at most countably infinite with the only accumulation point at zero and most importantly, the eigenfunctions form an orthonormal basis for the range of \bar{R} . Thus, the POD basis of dimension r corresponds to a set of r dominant eigenfunctions.

Note that in practice, it is computationally advantageous to compute this basis from a singular value decomposition (SVD) of the data:

$$\mathbf{y}(x, t) = \sum_{j=1}^{\infty} \phi_j(x) \underbrace{\sigma_j \psi_j(t)}_{\bar{a}_j(t)}$$

where the POD basis corresponds to the dominant (left) singular vectors and the effectiveness of the basis is usually measured by the following best approximation property of the SVD

$$(8) \quad \frac{1}{T} \int_0^T \left\| \mathbf{y}(\cdot, t) - \sum_{j=1}^r \phi_j \bar{a}_j(t) \right\|^2 dt = \sum_{j=r+1}^{\infty} \sigma_j^2.$$

One measure of the effectiveness of POD is related to the rate of decay of the singular values and the POD energy is measured as

$$E_r = \frac{\sum_{j=1}^r \sigma_j^2}{\sum_{j=1}^{\infty} \sigma_j^2}.$$

For the purposes of our discussion of the principal interval decomposition in the next section, we point out that a third, equivalent characterization of POD is

$$(9) \quad \phi_1 = \min_{\|\phi\|=1} \left\{ \frac{1}{T} \int_0^T \|\mathbf{y}(\cdot, t) - \phi(\cdot) \bar{a}(t)\|^2 dt \right\}$$

subject to the constraint that

$$(10) \quad \bar{a}(t) = (\mathbf{y}(\cdot, t), \phi(\cdot)).$$

Subsequent basis elements are defined as

$$\phi_m = \min_{\|\phi\|=1, \phi \perp P^{m-1}} \left\{ \frac{1}{T} \int_0^T \left\| \mathbf{y}(\cdot, t) - \sum_{j=1}^m \phi_j(\cdot) \bar{a}_j(t) \right\|^2 dt \right\}$$

with

$$\bar{a}_j(t) = (\mathbf{y}(\cdot, t), \phi_j(\cdot)), \quad j = 1, \dots, m.$$

We now make a few remarks about the POD basis

- The POD preserves linear properties. Specifically, for the fluid flow applications we consider,
 - If $\nabla \cdot \mathbf{y} = 0$, then $\nabla \cdot \phi_j = 0$ for $j = 1, \dots, r$. In other words, $P^r \subset \mathbf{X}_{\text{div}}$.
 - If $\mathbf{y}|_{\Gamma_1} = 0$ (with $\Gamma_1 \subseteq \partial\Omega$), then $\phi_j|_{\Gamma_1} = 0$.
- The best approximation result quoted in (8) is only an estimate of how a reduced-order model will perform in practice. Rather than

$$\mathbf{u}(x, t) = \mathbf{c}(x, t) + \sum_{j=1}^r \phi_j(x) \bar{a}_j(t),$$

the reduced-order model will actually be

$$\mathbf{u}(x, t) = \mathbf{c}(x, t) + \sum_{j=1}^r \phi_j(x) a_j(t),$$

with $\mathbf{a} = \{a_j\}_{j=1}^r$ coming from a dynamical system such as (6).

This last comment emphasizes that POD does not lead to the best possible basis for reduced-order modeling. In fact, the construction of optimal bases has been the subject of a number of recent studies [2, 32]. These improvements, however, require a lot of computation as well as special treatment to ensure that the linear properties discussed above are preserved.

In the next section, we discuss alternate reduced-order modeling strategies that are built upon the optimization problem described in (9) and (10) above.

3. Principal interval decomposition and extensions

One limiting factor in using the POD basis is that time averaging can smooth out information that is only expressed over small intervals of time. It is well known that POD is not very effective for convective flows for this reason. For example, consider the solution to the one-way wave equation

$$u_t + u_x = 0 \quad \text{with} \quad u(x, 0) = u_0(x) = e^{-x^2} \quad \text{over } \mathbb{R} \times \mathbb{R}.$$

The closed-form solution to this problem is $u(x, t) = u_0(t - x)$. In this case, the spatial autocorrelation function is

$$\begin{aligned} TR^s(x, \bar{x}) &= \int_{-T/2}^{T/2} e^{-(x-t)^2} e^{-(\bar{x}-t)^2} dt \\ &= \sqrt{\frac{\pi}{2}} e^{-(x-\bar{x})^2/2} \left(\operatorname{erf}\left(\frac{T-x-\bar{x}}{\sqrt{2}}\right) + \operatorname{erf}\left(\frac{T+x+\bar{x}}{\sqrt{2}}\right) \right). \end{aligned}$$

As we consider the solution over increasing time intervals, it tends to a *homogeneous function* in the limit (i.e., R^s can be expressed as $f(x - \bar{x})$). When this happens,

$$R^s(x, \bar{x}) = f(x - \bar{x}) = \sum_{k=-\infty}^{k=\infty} \lambda_k e^{2\pi i k(x-\bar{x})} = \sum_{k=-\infty}^{k=\infty} \lambda_k e^{2\pi i k x} e^{-2\pi i k \bar{x}}.$$

It can be seen that the POD vectors are the Fourier eigenfunctions [13]. Note that this is independent of $u_0(\cdot)$ and thus, the POD basis contains no information from the solution. When the POD has no correlation with the solution, obtaining a good low-dimensional reduced-order model may not be possible. This analysis can be used to explain the POD obtained for a solution to Burgers equation

$$u_t + uu_x = \epsilon u_{xx} \quad \text{with} \quad u(x, 0) = \begin{cases} 1 & x < 0.5 \\ 0 & x \geq 0.5 \end{cases} \quad \text{over } (0, 1) \times (0, T)$$

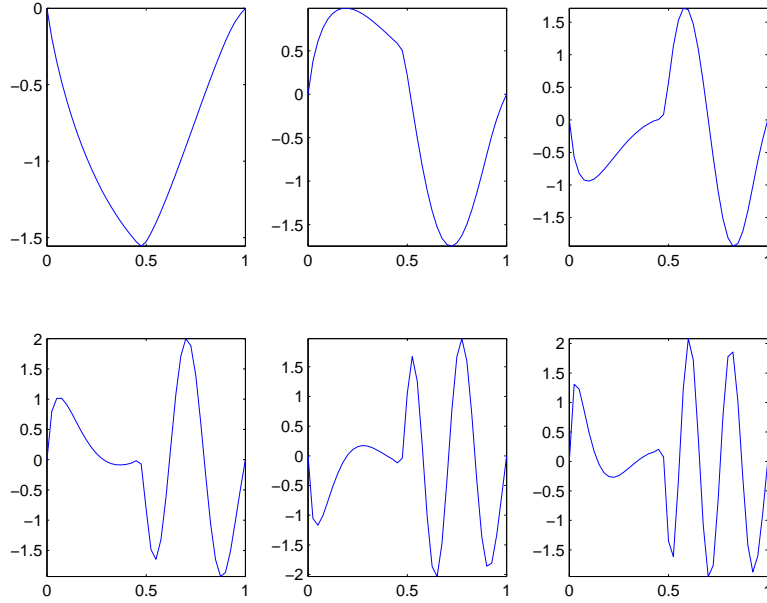


FIGURE 1. First six POD vectors for Burgers equation

and zero Dirichlet boundary conditions. Given the time snapshots for a simulation out to $T = 1$, we compute POD vectors and plot the dominant six in Figure 1. Recall that the simulation for this case consists of a falling wave over the left half of the domain and a traveling wave over the right half of the domain. This fact is seen in the POD basis. There is a lot of structure in the basis functions over the left half of the domain $[0, 0.5]$ while the right half $[0.5, 1]$ is primarily Fourier modes that become highly oscillatory as new POD basis functions are added.

3.1. The principal interval decomposition. One remedy for this challenge was suggested by IJzerman [16] and is known as the *principal interval decomposition* (PID). The idea is to partition the time interval $[0, T] = \cup_{i \in I} [t_i, t_{i+1}]$ into non-overlapping time intervals and computing the dominant POD basis element over each subinterval. A partition of the time interval enables us to impose extra constraints on the problem. A natural choice is to specify the relative error (ϵ) in the best approximation

$$\frac{1}{T} \int_0^T \|\mathbf{y}(\cdot, t) - \phi^{[t_i, t_{i+1}]}(\cdot) \bar{a}^{[t_i, t_{i+1}]}(t)\|^2 dt \leq \epsilon \frac{1}{T} \int_0^T \|\mathbf{u}(\cdot, t)\|^2 dt.$$

The basis and time coefficient function change with t . Naturally, there is a relationship between ϵ and the number of subintervals that are required to satisfy the tolerance.

To simplify the solution to this problem, this error condition is imposed over each subinterval

$$(11) \quad \int_{t_i}^{t_{i+1}} \|\mathbf{y}(\cdot, t) - \phi^{[t_i, t_{i+1}]}(\cdot) \bar{a}^{[t_i, t_{i+1}]}(t)\|^2 dt \leq \epsilon \int_{t_i}^{t_{i+1}} \|\mathbf{u}(\cdot, t)\|^2 dt.$$

Since this estimate is easy to satisfy over small time intervals, the PID algorithm is implemented by performing POD over increasing numbers of snapshots until this estimate is violated. Then, with the largest possible time interval over which the

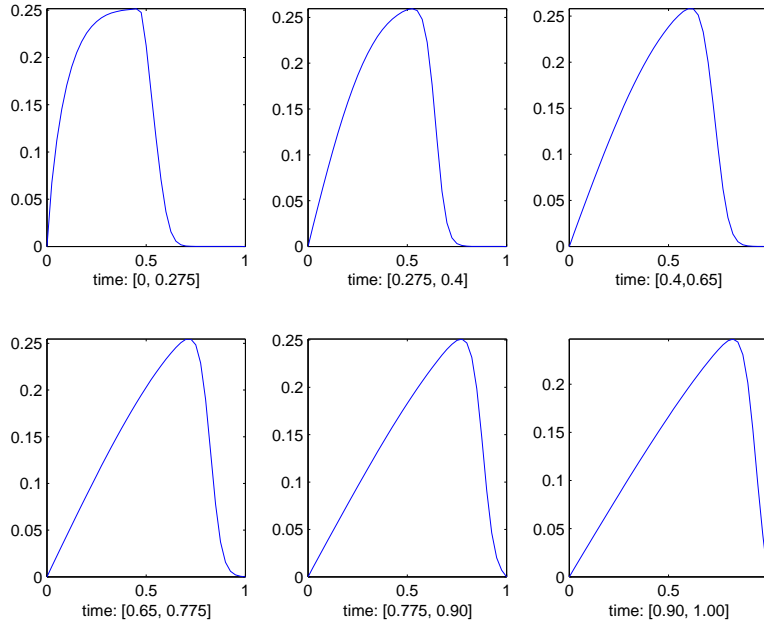


FIGURE 2. First six PID vectors for Burgers equation

estimate holds, the current PID vector and interval are stored, and the algorithm continues. The best possible choices for ϵ are those for which any smaller value increases the number of required subintervals.

The PID vectors and time intervals for the Burgers equation example above are displayed in Figure 2. These PID vectors are very similar to individual time snapshots. Thus, one can interpret PID as a method for doing weighted time-sampling of the simulation snapshots. In this sense, it is related to other sampling strategies, such as CVT reduced-order modeling methods [5]. As ϵ is decreased, every discrete time snapshot is selected as a PID basis vector valid over an interval of length Δt .

We make two remarks about the PID as described above. First of all, since the PID is in essence a POD applied to subsets of snapshots in the input collection, the PID basis functions also preserve linear properties of the collection. Thus, for Navier-Stokes simulations, they are divergence free, etc. Secondly, there are efficient algorithms to update an existing SVD when column vectors are added to the original matrix. The PID is obtained by taking the SVD of smaller matrices than the POD, however, this is done many more times. We did not have any need to exploit the computational efficiency of an SVD updating strategy for any of the problem sizes considered in this paper, but this may be required for larger problems.

3.2. Extensions. There are three natural extensions to the PID that we will consider in this work. The first is the possibility of using more than one PID function per interval. Thus, the reduced-order model would be of the general form

$$(12) \quad \mathbf{u}^r(x, t) = \mathbf{c}(x, t) + \sum_{j=1}^{r_i} \phi_j^{[t_i, t_{i+1}]}(x) a_j^{[t_i, t_{i+1}]}(t)$$

for each interval $t \in [t_i, t_{i+1}]$. Although this extension would allow the possibility to adaptively determine the benefit of increasing the dimension of the basis in each time subinterval, we will explore this trade-off for fixed basis size.

One difficulty in using a reduced-order model of the form (12), even with $r_i = 1$, is determining good initial conditions, $a_j^{[t_i, t_{i+1}]}(t_i)$, when switching models. Thus, one could consider adding basis elements from nearby subintervals,

$$\begin{aligned}
 \mathbf{u}^r(x, t) = \mathbf{c}(x, t) &+ \sum_{j=1}^{r_{i-1}} \phi_j^{[t_{i-1}, t_i]}(x) a_j^{[t_{i-1}, t_i]}(t) \\
 (13) \qquad \qquad \qquad &+ \sum_{j=1}^{r_i} \phi_j^{[t_i, t_{i+1}]}(x) a_j^{[t_i, t_{i+1}]}(t) \\
 &+ \sum_{j=1}^{r_{i+1}} \phi_j^{[t_{i+1}, t_{i+2}]}(x) a_j^{[t_{i+1}, t_{i+2}]}(t),
 \end{aligned}$$

over the time interval $t \in [t_i, t_{i+1}]$. The advantage is that there are $r_{i-1} + r_i$ common basis elements in the adjacent time intervals $[t_{i-1}, t_i]$ and $[t_i, t_{i+1}]$.

A third extension replaces the condition (11) with the condition

$$\int_{t_i}^{t_{i+1}} \|\mathbf{y}(\cdot, t) - \phi(\cdot)\mathbf{a}(t)\|^2 dt \leq \epsilon \int_{t_i}^{t_{i+1}} \|\mathbf{u}(\cdot, t)\|^2 dt,$$

where \mathbf{a} is determined from the reduced-order model (6). The advantage of this approach is that we replace the heuristic in (11) with a better representation of the actual reduced-order modeling error.

Note that we could combine any of these extensions. However, for this study, we consider their advantages separately.

4. Numerical experiments

We test the proposed reduced-order modeling strategies on a two-dimensional flow consisting of vortex shedding past a square cylinder. This example has been used in recent reduced-order modeling studies for fluids [6, 9]. We describe our snapshot generation below, followed by comparisons of POD and PID bases and reduced-order model simulations.

4.1. Flow description and computational simulation. Two-dimensional flow over a square cylinder is used to test our models. At a Reynolds number of 100 based on the square edge length and the freestream velocity, this flow is known to be laminar and unsteady, exhibiting a von Karman vortex street [27]. Our computational domain is based on the study of Hristova [15]: the inflow and sides of the computational domain are located six edge lengths away, while the outflow boundary is placed fifteen edge lengths away. The mesh is defined by an adaptive refinement procedure on the steady-state equations with additional uniform refinement in the wake region. The final mesh for unsteady calculations contains 21626 nodes and 7152 elements. An implicit Euler time stepping scheme with $\Delta t = 0.00945$ is used.

In the present computation, the Strouhal number,

$$St \equiv \frac{fD}{U_\infty}$$

(D -length of square side, f -measured shedding frequency, U_∞ -inflow velocity) was computed as 0.14781. This compares well to published experimental and numerical values of 0.138 (Okajima [27]), 0.139 (Breuer et al. [4]), 0.150 (Davis et al.[7]),

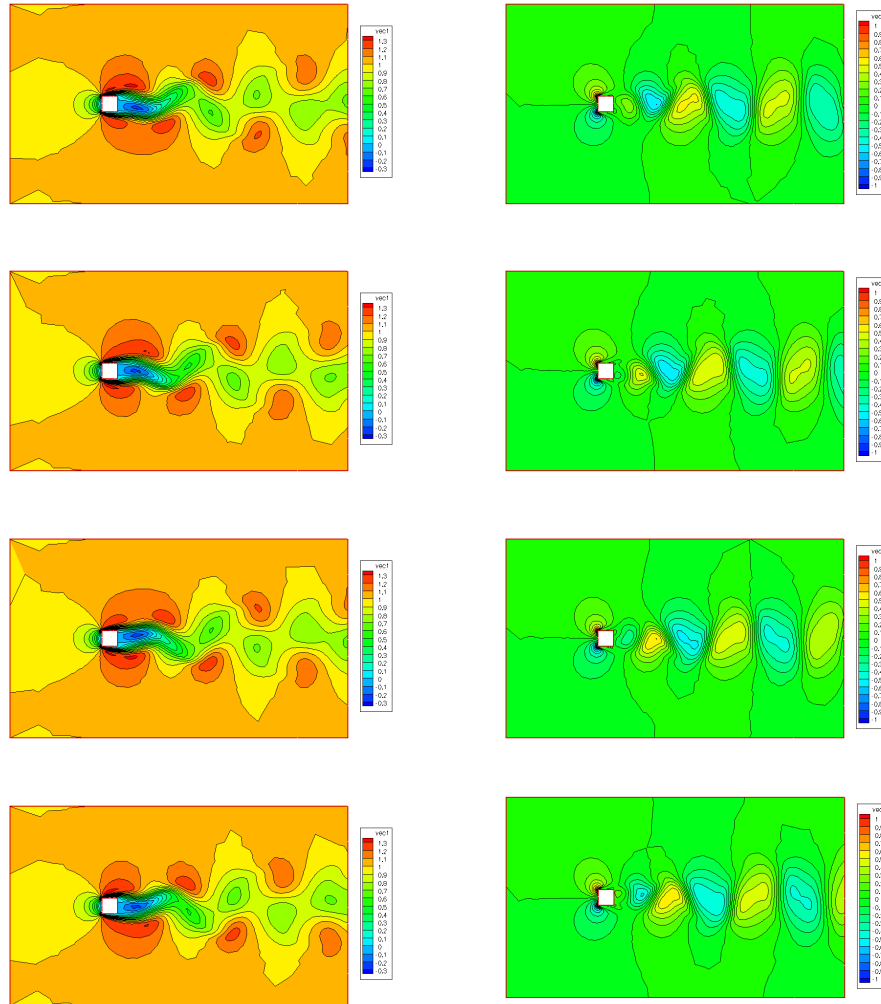


FIGURE 3. Contours of Horizontal and Vertical Velocity Components

and 0.152 (Saha et al.[30]). After an initial settling time, 60 snapshots of the solution over one period were collected to develop a reduced-order model (every 12 timesteps). This is a fairly minimal sampling (for example, 480 snapshots over one period were used in [6]) and does lead to low resolution of the length of the PID time intervals. However, as we shall see, this coarse sampling is enough to produce good models. Contours of the velocity components for four representative snapshots equally spaced over one shedding period are shown in Figure 3.

4.2. Reduced-order bases. These sixty snapshots over one shedding period were used to generate six POD vectors. The time-average of the flow was taken as the centering trajectory \mathbf{c} . Thus, all of the POD vectors should have zero Dirichlet boundary conditions and zero normal stresses. Contours of the first, third and fifth POD vectors are shown in Figure 4. The second, fourth and sixth vectors

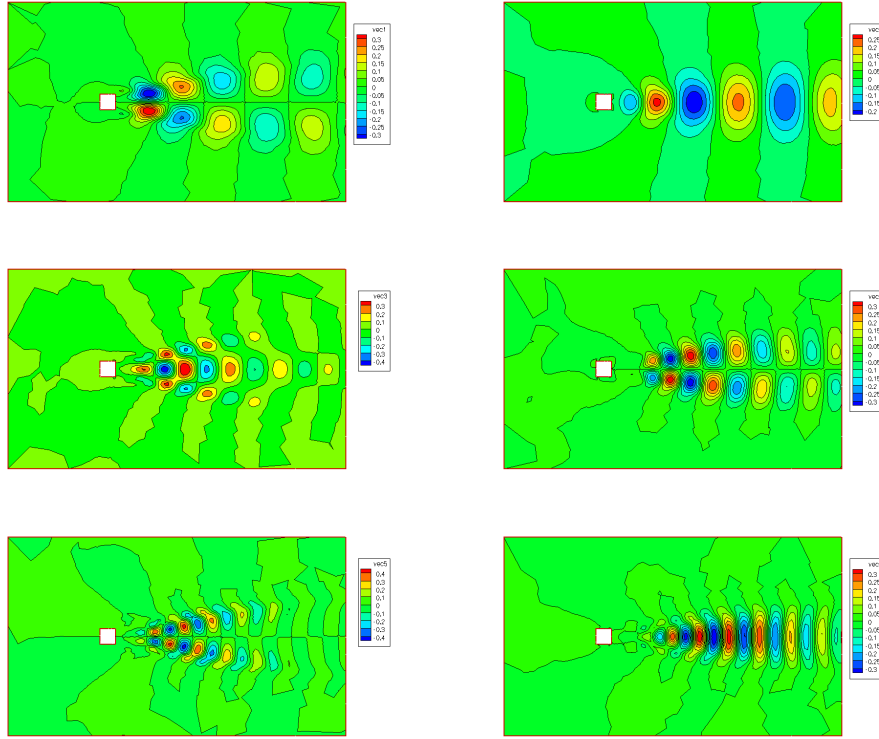


FIGURE 4. Contours of horizontal and vertical POD vector fields

are similar. The vectors either symmetric or antisymmetric and the singular values decay pairwise, reflecting the problem symmetry (also seen in [6]).

These first six vectors contain over 99% of the POD energy. As a benchmark, the corresponding reduced-order model was integrated for the time required to complete one shedding cycle. The coefficients are plotted in Figure 5. Notice that there is a loss of energy in the system (more pronounced with higher frequency modes). The error in the ROM (computed with trapezoidal integration) is

$$\int_{170.56}^{177.25} \|\mathbf{u}(\cdot, t) - \mathbf{u}^r(\cdot, t)\|^2 dt = 13.31, \quad \text{with} \quad \int_{170.56}^{177.25} \|\mathbf{u}(\cdot, t)\|^2 dt = 2511.06.$$

The relative error in the vertical component v is high, however, at nearly 25%.

We then specify $\epsilon=4.52e-2$ and obtain six PID vectors and intervals. We display three of these in Figure 6. Notice that unlike the Burgers equation example, these PID vectors do not look very similar to the corresponding simulation snapshots seen in Figure 3. As noted above, the singular values tend to drop off pairwise. Thus, it makes sense to consider the extension to several PID vectors per interval as discussed in the previous section. We further note that the model generated with these six PID vectors and intervals alone produced a much worse fit to data,

$$\int_{170.56}^{177.25} \|\mathbf{u}(\cdot, t) - \mathbf{u}^r(\cdot, t)\|^2 dt = 34.72.$$

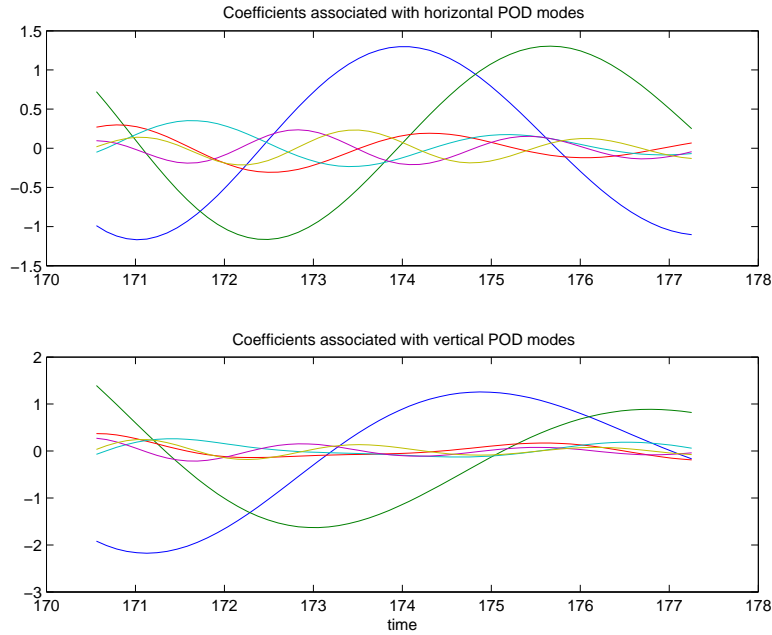


FIGURE 5. Coefficients of POD/Galerkin Reduced-Order Model

The relative error in the vertical velocity component is over 50%. This is not surprising since this problem was not designed to demonstrate the advantages of the PID.

4.3. Test of PID extensions. This example of flow past a square cylinder used to demonstrate three PID extensions discussed in Section 3.2.

4.3.1. Increasing dimension of PID basis. To test our first extension, we computed the best PID relative error tolerance, ϵ from equation (11), with varying PID basis dimension r and number of PID intervals N . The results from our study appear in Table 1. It was not possible to find a value of ϵ corresponding to $r = 1$ and $N = 2$ since the maximum error occurred at the 31st snapshot in the $r = 1$ and $N = 1$ case. In many of our cases, the time intervals were equally distributed over the shedding period. Those that were not are denoted with a (*) beginning with $r = 3$ and $N = 5$. There is a large sensitivity of the subdivision into time intervals as the performance requirement increases. This is partly due to the use of a small number of time samples (in the $r = 6$ and $N = 6$ case, there are 36 basis functions from 60 snapshots). Also note that there was no effort made to optimize these parameters by considering cyclic permutations of the time snapshots (time intervals could perhaps be lengthened by considering the adequacy of basis elements in $[t_{N-1}, 177.25]$ to represent data in $[170.56, t_1]$). Thus, the values of ϵ could be lowered, especially in the non-uniform (*)-ed cases.

Note that there is better performance when bases are introduced in pairs. This is observed in Table 1 by looking at the decrease of ϵ in columns (constant N). The biggest improvement occurs when going from $r = 1$ to $r = 2$.

The first column in Table 1 corresponds to the relative approximation error associated with standard POD. Singular vectors are computed using `svd(Y,0)`; in MATLAB. The singular values decay in pairs and very fast for this problem. For

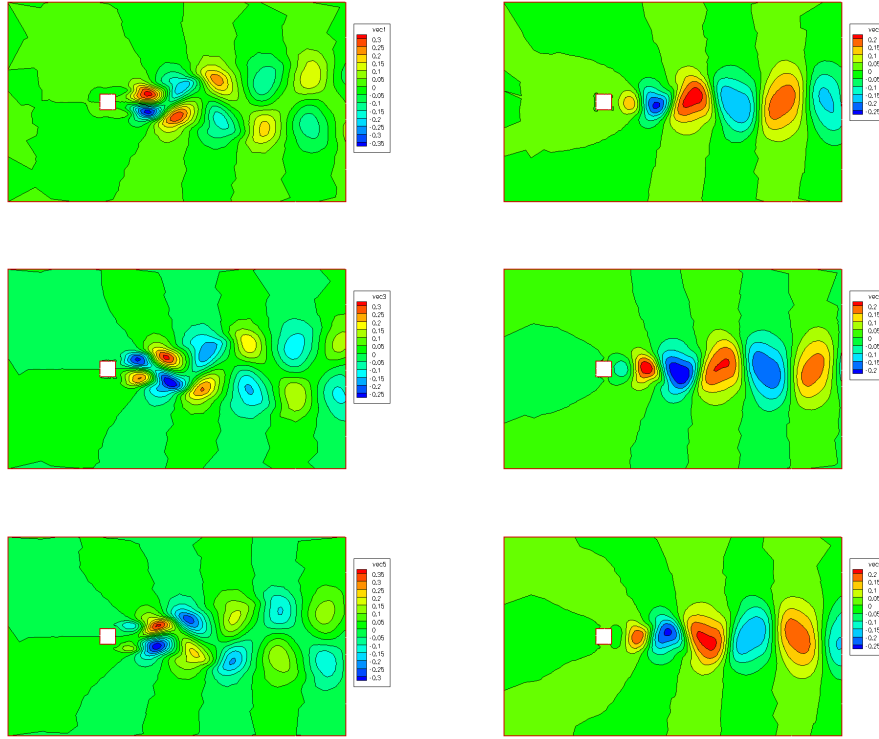


FIGURE 6. Contours of 1st, 3rd and 5th PID vector fields

TABLE 1. Optimal ϵ for varying basis size (r) and intervals (N)

$r \setminus N$	1	2	3	4	5	6
1	1.02e-2	*	6.52e-3	4.18e-3	2.86e-3	2.06e-3
2	8.95e-4	6.21e-4	3.04e-4	1.40e-4	6.84e-5	3.69e-5
3	5.92e-4	2.69e-4	7.58e-5	2.67e-5	9.93e-6*	5.73e-6*
4	2.96e-4	5.58e-5	1.21e-5	7.27e-6*	3.94e-6*	3.19e-6*
5	1.59e-4	4.58e-5	1.85e-5	1.32e-5*	1.01e-5*	9.47e-6*
6	6.43e-5	5.24e-5	2.09e-5*	1.47e-5*	1.12e-5*	9.71e-6*

many problems involving flows, they do not decrease as quickly. Thus, at some point, the best strategy to improve the performance of a reduced-order model is to introduce sub-intervals. The best estimate we were able to achieve is for $r = 4$ and $N = 6$.

While more intervals lead to better performance, at the same level of reduction, there is a computational cost associated with this. For our Navier-Stokes predictions, the majority of the work needed to simulate (6) can be performed upfront by precomputing integrals such as $(\phi_j \cdot \nabla \phi_i, \phi_k)$. The final system is r dimensional and can be simulated very cheaply. This upfront integration cost needs to be spent for each time interval and should be considered when weighing the benefits of PID.

4.3.2. Using neighboring vectors to simulate PID. Note that the value of ϵ in the PID estimate is a heuristic. There are two facts that need to be considered. The first is the natural error in the interpolation of the solution at the end of one interval onto a basis for the current interval. One of the extensions in Section 3.2 suggested a practical means to address this. The second fact is that the model actually uses an \mathbf{a} from the model coefficients (6) instead of the projection $\bar{\mathbf{a}}$. This discrepancy is considered in the next section.

Our numerical experiment compares six dimensional models for the square cylinder flow. As noted earlier, the error in the six dimensional POD reduced-order model is

$$\int_{170.56}^{177.25} \|\mathbf{u}(\cdot, t) - \mathbf{u}^r(\cdot, t)\|^2 dt = 13.31$$

corresponding to a relative error of 5.30e-3 (compared with the predicted error of 6.43e-5 when the ideal coefficient function is used). The PID model we consider uses two PID vectors over six intervals ($r = 2$, $N = 6$) to generate the basis. When we build our model, we use six basis vectors over each time interval. These correspond to the current, previous and next intervals as indicated in (13). Note that for the first and last interval, we take advantage of the fact that we have a periodic problem (otherwise, we could reduce the dimension of the overall model at the ends, or add more basis elements to keep the dimension the same). For this reduced-order model, we obtain an error of

$$\int_{170.56}^{177.25} \|\mathbf{u}(\cdot, t) - \mathbf{u}^r(\cdot, t)\|^2 dt = 12.70.$$

As we expected, this offers an improvement over POD of the same dimension.

4.3.3. Using actual coefficients. In this final experiment, we demonstrate the construction of a PID with an actual error bound. As seen in the experiment above, the prediction given by *best approximation* arguments can be off by several orders of magnitude in practice. In many instances it may be desirable to build the model with a more accurate estimate of the model error (for example, optimization algorithms may be designed to take advantage of variable fidelity models, but require a proper hierarchy of models). Thus, we replace the $\bar{\mathbf{a}}$ in the PID tolerance with the value of \mathbf{a} obtained by the model equations (6). Note that we account for the errors in the projection, but models cannot be generated to an arbitrary accuracy.

This is a very expensive modification since the model equations are built and integrated every time the snapshot matrix is updated. We specified an exact relative error tolerance of $\epsilon=3.4e-4$ and chose to use two PID vectors per interval $r = 2$ which seems advantageous from our Table 1. Note that this specification would ideally lead to three intervals based on the *best approximation* coefficients. In the actual experiment, we came up with six, nearly equi-length intervals. The model with one interval has one interval that is shortened by one time step and another one that is lengthened by one time step.

5. Conclusions and future work

In this paper, we described the principal interval decomposition, which was initially developed by IJzerman [16]. We also presented a number of natural extensions. The most practical are the incorporation of multiple basis functions per interval and the use of neighboring basis information to minimize interpolation errors between intervals. This decomposition method was tested on a fluid flow problem consisting of flow past a square cylinder that is frequently used to validate

reduced-order models. Our extension, using two basis functions per interval and improving interpolation lead to a improvement over a standard POD model of the same dimension. While this problem clearly benefits from the use of pairs of basis functions, it was not designed explicitly to exploit some of the challenges with POD (for example, a pure traveling wave problem). Future numerical experiments will be performed to better illustrate this advantage of the PID.

Note that one may consider alternative approaches to build models that can predict nearby flow behavior. For example, the nearby flow approximation given in [12] uses sensitivity analysis, e.g. [3], to find rapid estimations of nearby flows. This is not practical in flows that evolve in time. However, it may be feasible to build sensitivity analysis into POD input collections to make bases that are more suitable to parameter variations. This will be investigated in future work.

References

- [1] A.C. Antoulas. *Approximation of Large-Scale Dynamical Systems*. Advances in Design and Control. SIAM, Philadelphia, 2005.
- [2] J. Borggaard. Optimal reduced-order modeling for nonlinear distributed parameter systems. In *2006 American Control Conference*, 2006. Paper WeB13.3.
- [3] J. Borggaard, J. Burns, E. Cliff, and M. Gunzburger. Sensitivity calculations for a 2D, inviscid, supersonic forebody problem. In H. T. Banks, R. Fabiano, and K. Ito, editors, *Identification and Control of Systems Governed by Partial Differential Equations*, pages 14–24, Philadelphia, PA, 1993. SIAM Publications.
- [4] M. Breuer, J. Bernsdorf, T. Zeiser, and F. Durst. Accurate computation of the laminar flow past a square cylinder based on two different methods: Lattice-Boltzmann and finite volume. *International Journal of Heat and Fluid Flow*, 21:186–196, 2000.
- [5] J. Burkardt, Q. Du, M. Gunzburger, and H.-C. Lee. Reduced order modeling of complex systems. In *Proc. 20th Biennial Conference on Numerical Analysis*, pages 29–38, 2003.
- [6] M. Couplet, C. Basdevant, and P. Sagaut. Calibrated reduced-order POD-Galerkin system for fluid flow modeling. *Journal of Computational Physics*, 207(1):192–220, 2005.
- [7] R.W. Davis, E.F. Moore, and L.P. Purtell. A numerical-experimental study on confined flow around rectangular cylinders. *Physics of Fluids*, 23:46–59, 1984.
- [8] M.Ö. Efe and H. Özbay. Low dimensional modelling and Dirichlet boundary controller design for Burgers equation. *International Journal of Control*, 44(10):895–906, 2004.
- [9] B. Galletti, C.H. Bruneau, L. Zannetti, and A. Iollo. Low-order modelling of laminar flow regimes past a confined square cylinder. *Journal of Fluid Mechanics*, 503:161–170, 2004.
- [10] S. Ganapathysubramanian and N. Zabaras. Design across length scales: A reduced-order model of polycrystal plasticity for the control of microstructure-sensitive material properties. *Computation Methods in Applied Mechanics and Engineering*, 193:5017–5034, 2004.
- [11] M. Gunzburger. *Finite Element Methods for Viscous Incompressible Flows: A Guide to Theory, Practice and Algorithms*. Academic Press, 1989.
- [12] M. Gunzburger. *Perspectives in Flow Control and Optimization*. SIAM, 2002.
- [13] P. Holmes, J.L. Lumley, and G. Berkooz. *Turbulence, Coherent Structures, Dynamical Systems and Symmetry*. Cambridge University Press, 1996.
- [14] H. Hotelling. Analysis of a complex of statistical variables with principal components. *Journal of Educational Psychology*, 24:417–441, 1933.
- [15] H. Hristova. Analyse de sensibilité d'écoulements instationnaires visqueux laminaires. Master's thesis, École Polytechnique de Montréal, 2003.
- [16] W.L. IJzerman. *Signal representation and modeling of spatial structures in fluids*. PhD thesis, Universiteit Twente, 2000.
- [17] K. Ito and S.S. Ravindran. A reduced-order method for simulation and control of fluid flows. *Journal of Computational Physics*, 143(2):403–425, 1998.
- [18] D.A. Jones, L.G. Margolin, and E.S. Titi. On the effectiveness of the approximate inertial manifold—a computational study. *Theoretical and Computational Fluid Dynamics*, 7:243–260, 1995.
- [19] K. Karhunen. Zur spektraltheorie stochastischer prozesse. *Annales Academiae Scientiarum Fennicae*, 37, 1946.
- [20] D. Kovacs. Inertial manifolds and nonlinear Galerkin methods. Master's thesis, Virginia Tech, 2005.

- [21] K. Kunisch, S. Volkwein, and L. Xie. HJB-POD-based feedback design for the optimal control of evolution problems. *SIAM Journal on Applied Dynamical Systems*, 3(4):701–722, 2004.
- [22] M. Loève. *Probability Theory*. Van Nostrand, New York, 1955.
- [23] E.N. Lorenz. Empirical orthogonal functions and statistical weather prediction. Technical report, M.I.T., 1956.
- [24] M. Marion and R. Temam. Nonlinear Galerkin methods. *SIAM Journal of Numerical Analysis*, 26(5):1139–1157, 1989.
- [25] B. Noack, G. Tadmor, and M. Morzyński. A hierarchy of low-dimensional models for the transient and post-transient cylinder wake. *J. Fluid Mechanics*, 497:335–363, 2003.
- [26] B.R. Noack and H. Eckelmann. A low-dimensional Galerkin method for the three-dimensional flow around a circular cylinder. *Physics of Fluids*, 6:124–143, 1994.
- [27] A. Okajima. Strouhal number of rectangular cylinders. *Journal of Fluid Mechanics*, 123:379–398, 1982.
- [28] J.S. Peterson. The reduced basis method for incompressible viscous flow calculations. *SIAM Journal on Scientific and Statistical Computing*, 10(4):777–786, 1989.
- [29] C.W. Rowley and D.R. Williams. Dynamics and control of high-Reynolds-number flow over open cavities. *Annual Review of Fluid Mechanics*, 38:251–276, 2006.
- [30] A.K. Saha, G. Biswas, and K. Muralidhar. Three-dimensional study of flow past a square cylinder at low Reynolds numbers. *International Journal of Heat and Fluid Flow*, 24:54–66, 2003.
- [31] S. Sirisup and G.E. Karniadakis. A spectral viscosity method for correcting the long-term behavior of POD models. *Journal of Computational Physics*, 194:92–116, 2004.
- [32] K. Willcox, O. Ghattas, B. van Bloemen Waanders, and B. Bader. An optimization framework for goal-oriented, model-based reduction of large-scale systems. In *Joint 44th IEEE CDC and ECC conference*, Seville, Spain, 2005.
- [33] K. Willcox and A. Megretski. Fourier series for accurate, stable, reduced-order models in large-scale linear applications. *SIAM Journal on Scientific Computing*, 26(3):944–962, 2005.

Interdisciplinary Center for Applied Mathematics, Virginia Tech, Blacksburg, VA 24061, USA

E-mail: jborggaard@vt.edu

URL: <http://www.icam.vt.edu/people/borggaard>

Génie mécanique, École Polytechnique de Montréal, Montréal, QC H3C 3A7, Canada

E-mail: Alexander.Hay@polymtl.ca and Dominique.Pelletier@polymtl.ca

URL: <http://www.polymtl.ca/recherche/rc/en/professeurs/details.php?NoProf=230>